Laboratory validation of SWASH longshore current modelling

Zhang, Rong; Zijlema, Marcel; Stive, Marcel

DOI
10.1016/j.coastaleng.2018.10.005

Publication date
2018

Document Version
Final published version

Published in
Coastal Engineering

Citation (APA)
Zhang, R., Zijlema, M., & Stive, M. (2018). Laboratory validation of SWASH longshore current modelling. *Coastal Engineering*, *142*, 95-105. https://doi.org/10.1016/j.coastaleng.2018.10.005

Coastal Engineering 142 (2018) 95–105

Contents lists available at ScienceDirect

Coastal Engineering

journal homepage: www.elsevier.com/locate/coastaleng

Laboratory validation of SWASH longshore current modelling

Rong Zhang*, Marcel Zijlema, Marcel J.F. Stive

Department of Hydraulic Engineering, Delft University of Technology, Delft, the Netherlands

ARTICLE INFO

Keywords:
Longshore current
SWASH
Numerical modelling

ABSTRACT

In this paper, the ability of the numerical phase resolving model SWASH (Simulating WAves till SHore) to hindcast wave-induced longshore currents is evaluated. Using default settings for all processes modelled, highly accurate results are found for wave heights, mean water levels and longshore currents. While wave current interaction is intrinsically modelled, insights into the spatial variation of wave driven longshore currents are found. Additionally, vertical variations of modelled longshore currents have been compared. Depth uniform profiles of longshore current within surf zone are noted on plane beaches under regular waves, except for minor deviations near the shoreline. The apparent validity of a depth-uniform longshore current encourages the use of a depth-averaged moment balance equation to compute the longshore current. A simpler model is shown to also be able to predict a proper magnitude of longshore current, although the cross-shore distribution – in contrast with SWASH - needs tuning for the eddy viscosity and the bottom friction coefficient, since the distribution of the wave-induced longshore current heavily depends on lateral mixing.

1. Introduction

Longshore currents, generated by obliquely incident breaking waves, play an important role in driving longshore sediment transport and in changing coastal morphology. The theory of longshore currents has progressed importantly (Bowen, 1969; Longuet-Higgins, 1970a,b; Thornton and Guza, 1986), since the concept of radiation stress was introduced (Longuet-Higgins and Stewart, 1964; Longuet-Higgins, 1970a,b). Among the proposed mathematical models, the simplest model is a 1D model based on momentum flux balance in alongshore direction on a planar beach under monochromatic wave incidence. In steady state and water depth averaged mode, the longshore current driving force is balanced by bottom friction and lateral friction. Although the average longshore current velocity across the entire surf zone could be properly predicted, the exact cross-shore distribution of the longshore current is more difficult to derive, since it highly depends on less-known lateral mixing mechanisms.

To investigate longshore current mechanisms, field investigations and laboratory experiments have been carried out. Earlier measurements are often limited to longshore maximum velocity or average velocity across the entire width of the surf zone, which does not reveal the cross-shore distribution of longshore current. The known first cross-shore distribution of longshore current was measured by Galvin and Eagleson (1964) along several shore normal profiles. These pioneering data are used widely to test longshore current theories. However, possible non-uniformity of the longshore current along the beach should be carefully considered (Visser, 1991). To avoid non-uniformity of the longshore current, well controlled, highly representative laboratory experiments were conducted by Visser (1980,1982,1984a,1984b,1991). Visser found that a virtually uniform longshore current is realized when the return flow in the offshore region of the wave basin is minimal. Therefore, Visser introduced an active external recirculation system driven by pumps to minimize the circulation flow in the wave basin. Because of the well-controlled uniformity of the longshore current, this data set has been used as a benchmark set for developing longshore current theories and validating numerical models (e.g. Smith et al., 1993; Svendsen and Putrevu, 1994; Chen, 2003; Rijnsdorp et al., 2017; Hsu et al., 2017). This experimental example setup, guaranteeing the production of an alongshore uniform longshore current in the laboratory, was also adopted by Hamilton and Ebersole (2001). In addition, a unique, unexplored and unpublished data set produced by large-scale, outdoor laboratory experiments (Hulsbergen and ter Horst, 1973) is presented and shown to be a worthy, additional dataset for validation. Other than the previously mentioned experiments investigating wave-induced longshore currents on planar beaches, Reniers and Battjes (1997) carried out experiments which focused on longshore currents over more geographically complicated, barred beaches.

The measurements of longshore currents obtained from the above-mentioned experiments provide an excellent database to validate and/

* Corresponding author.
E-mail address: R.Zhang@tudelft.nl (R. Zhang).

https://doi.org/10.1016/j.coastaleng.2018.10.005
Received 22 April 2018; Received in revised form 28 September 2018; Accepted 13 October 2018
Available online 16 October 2018
0378-3839/

or calibrate numerical simulation models. The primary aim of this paper is to validate the ability to simulate the spatial variation of wave-driven longshore currents by the phase resolving, non-hydrostatic numerical model SWASH (Simulating Wave till SHore). Validation is preferred over calibration, since validation relies on default parameter settings while calibration relies on adjusted parameter settings for a specific dataset. A verified (validated or calibrated) model is useful to design hard and soft coastal interventions and/or instrument deployment in experiments. Additionally, a very simplified 1D model is introduced to explore the most basic physics behind wave-induced longshore currents.

In the present work, we set up the wave-flow model SWASH with default parameters to validate its ability to simulate wave-induced longshore currents on a laboratory scale. The governing equations of the SWASH model are listed in subsection 2.1. Then, a separate simplified depth averaged 1D model is demonstrated in subsection 2.2. The configurations of the chosen laboratory experiments are described in the following subsection 2.3. The results of SWASH modelling longshore currents are presented and compared to the 1D model results in Section 3. Finally, in Section 4 a discussion and in Section 5 conclusions are given.

2. Methods

2.1. Numerical model SWASH

SWASH (Zijlema et al., 2011) is a flow-wave model which can simulate unsteady, non-hydrostatic free-surface flow in the time-domain, having a wide application range in coastal waters. The governing equations are non-linear shallow water equations including non-hydrostatic effects. The local continuity equation and momentum equations in 3D configuration are given as

$$\frac{\partial u}{\partial x}+\frac{\partial v}{\partial y}+\frac{\partial w}{\partial z}=0 \tag{2.1}$$

$$\frac{\partial u}{\partial t}+\frac{\partial uu}{\partial x}+\frac{\partial uv}{\partial y}+\frac{\partial uw}{\partial z}+\frac{1}{\rho}\frac{\partial p_h+p_{nh}}{\partial x}=\frac{\partial \tau_{xx}}{\partial x}+\frac{\partial \tau_{xy}}{\partial y}+\frac{\partial \tau_{xz}}{\partial z} \tag{2.2}$$

$$\frac{\partial v}{\partial t}+\frac{\partial vu}{\partial x}+\frac{\partial vv}{\partial y}+\frac{\partial vw}{\partial z}+\frac{1}{\rho}\frac{\partial p_h+p_{nh}}{\partial y}=\frac{\partial \tau_{yx}}{\partial x}+\frac{\partial \tau_{yy}}{\partial y}+\frac{\partial \tau_{yz}}{\partial z} \tag{2.3}$$

$$\frac{\partial w}{\partial t}+\frac{\partial wu}{\partial x}+\frac{\partial wv}{\partial y}+\frac{\partial ww}{\partial z}+\frac{1}{\rho}\frac{\partial p_h+p_{nh}}{\partial z}+g=\frac{\partial \tau_{zx}}{\partial x}+\frac{\partial \tau_{zy}}{\partial y}+\frac{\partial \tau_{zz}}{\partial z} \tag{2.4}$$

Where u and v represent the horizontal velocity in x and y direction respectively, x is the direction normal to the shore, and y the direction parallel along the shore. The moving free surface $\zeta(x, y, t)$ and the stationary bottom z = -d(x,y) restrict the water column. The hydrostatic pressure is explicitly expressed as $p_h = \rho g(\zeta - z)$, so $\partial_x p_h = \rho g \partial_x \zeta$ (where ∂_x stands for ∂/∂_x), $\partial_y p_h = \rho g \partial_y \zeta$ and $\partial_z p_h = -\rho g$ (where g is the gravitational acceleration). p_{nh} is the non-hydrostatic pressure part. τ_{ij} are the turbulent stresses (where i or j denotes the coordinates). Equation (2.1) is the local continuity equation, and Equations (2.2)-(2.4) are momentum equations including the effects of mixing and external forces.

The kinematic boundary conditions at the free surface and bottom are

$$w|_{z=\zeta}=\frac{\partial \zeta}{\partial t}+u\frac{\partial \zeta}{\partial x}+v\frac{\partial \zeta}{\partial y} \tag{2.5}$$

$$w|_{z=-d}=-u\frac{\partial d}{\partial x}-v\frac{\partial d}{\partial y} \tag{2.6}$$

Integrating the local continuity Equation (2.1) with substituting kinematic boundary conditions at surface and bottom Equations. (2.5)–(2.6), a global continuity equation is induced

$$\frac{\partial \zeta}{\partial t}+\frac{\partial}{\partial x}\int_{-d}^{\zeta} u dz+\frac{\partial}{\partial y}\int_{-d}^{\zeta} v dz=0 \tag{2.7}$$

Where t is the time, ζ is the free surface elevation from still water level, z = -d is the bottom, d is the still water depth.

The dynamic boundary condition at the bottom is confined to bottom friction. The bottom friction stress is based on a quadratic friction law $\tau_b = C_f \frac{U|U|}{h}$, where $h = \zeta + d$ is the total water depth, U is the depth averaged velocity, and C_f is a dimensionless friction coefficient. At the free surface, zero atmospheric pressure ($p_h = p_{nh} = 0$) is assumed and no surface stresses are considered.

The turbulent stresses are given based on eddy viscosity closure equations. The horizontal viscosity and vertical viscosity are estimated by the Smagorinsky type model (Smagorinsky, 1963) and the k- ε model (Launder and Spalding, 1974), respectively.

For a comprehensive description of the SWASH model and its numerical schemes, reference is made to Zijlema et al. (2011), Smit et al. (2013) and Rijnsdorp et al. (2014). Extensive validations and applications of SWASH model can be found in the literature. For instance, Rijnsdorp et al. (2014) evaluated the ability of SWASH model to simulate infragravity wave dynamics and found a good agreement with flume observations. de Bakker et al. (2016) designed a numerical study using the SWASH model to investigate nonlinear energy transfers between waves, especially focusing on beach steepness effects on nonlinear infragravity wave interactions. Suzuki et al. (2017) validated the capability of SWASH model to estimate wave overtopping for impermeable coastal structures against physical model data.

2.2. 1D model

The depth averaged 1D model comprises a wave model and a current model. The wave model is based on the wave energy balance equation in the cross-shore direction including the wave roller effect, and the current model is based on the momentum balance equation in the alongshore direction. In contrast to the phase resolving SWASH model in multi-layered mode, the 1D model does not resolve the free flow surface, and the vertical flow structures. The 1D model thus is a very simplified model, expected however to include the basic physics behind the process of wave-induced currents. A comparison with the SWASH model will reveal whether including a physically more sophisticated approach is more robust.

2.2.1. Wave modelling

The governing equation determining the wave dynamics is the energy balance equation of wave energy:

$$\frac{d}{dx}(E_w c_g \cos\theta)=\varepsilon_w \tag{2.8}$$

where x is the shore normal direction, E_w is wave energy, ε_w is mean organised wave energy dissipation rate due to wave breaking and bottom friction. c_g is wave group velocity. Compared to dominant wave breaking dissipation, bottom frictional dissipation is negligible, except the very shallow run-up region (Thornton and Guza, 1983). For a monochromatic wave, using linear wave theory, the wave energy is expressed by the wave height:

$$E_w=\frac{1}{8}\rho g H^2 \tag{2.9}$$

and the group velocity c_g is described by

$$c_g = c\left(\frac{1}{2}+\frac{kh}{\sinh 2\,kh}\right) \tag{2.10}$$

The wave energy dissipation ε_w serves as a source term in the roller model (Stive and De Vriend, 1994)

$$-\varepsilon_w - \frac{d}{dx}(2E_r c\cos\theta) = c\tau_r \tag{2.11}$$

where τ_r is the shear stress between roller and water interface, for a steady roller it is given by Duncan (1981).

$$\tau_r = \rho_r g \sin\beta \frac{A}{L} \tag{2.12}$$

where A is cross-sectional area of the roller, β the slope of wave front, L wave length. ρ_r is density of the roller, generally less than undisturbed sea water for the entrainment of air at the aerated wave surface. Here, having $\rho_r \approx \rho$, to keep roller mass constant at a decrease in roller area A.

The second term of equation (2.9) is the gradient of roller energy flux, followed the definition by Svendsen (1984).

$$E_r = \frac{1}{2}\rho_r c^2 \frac{A}{L} \tag{2.13}$$

The wave height transformation proposed by Thornton and Guza (1983) is utilised. The wave dissipation is modelled by the classical periodic bore dissipation function as

$$\varepsilon_w = \frac{f}{4}\rho g \frac{(BH)^3}{h} \tag{2.14}$$

in which B expresses the deviation of wave breaking dissipation from bore dissipation.

For the ensemble, the average wave energy dissipation rate is calculated by

$$\varepsilon_w = \frac{\bar{f}}{4}\rho g \frac{B^3}{h}\int_0^\infty H^3 p_b(H)dH \tag{2.15}$$

where p_b is the probability density of breaking wave distribution.

The Thornton and Guza (1983) model modified the distribution of random wave heights from a Rayleigh distribution by a weighting function, the breaking wave dissipation is related to Hrms via:

$$\varepsilon_w = \frac{3\sqrt{\pi}}{16} B^3 \bar{f} \rho g \frac{H_{rms}^3}{h} M\left[1 - \frac{1}{\left(1 + \left(\frac{H_{rms}}{\gamma h}\right)^2\right)^{5/2}}\right] \tag{2.16}$$

$$M = 1 + tanh\left[8\left(\frac{H_{rms}}{\gamma h} - 1\right)\right] \tag{2.17}$$

Where H_{rms} is the root mean square wave height, and γ is the wave breaker index, B denotes the intensity of wave breaking, is usually the order of 1, but should be larger cause some researchers thought the classical hydraulic jump function underestimates the wave breaking dissipation (Thornton and Guza, 1983; Stive, 1984). According to the fitting of the model results to laboratory and field data by Thornton and Guza (1983), the range of calibrated value of B is between 0.8 and 1.7.

The wave radiation stress in the longshore direction is given by

$$S_{xy,w} = E_w \frac{c_g}{c}\cos\theta\sin\theta \tag{2.18}$$

Assuming a longshore uniform beach, the driving force of the wave-induced current is due to the cross-shore gradient of the longshore radiation shear stress, including the roller contribution:

$$F_y = -\frac{\sin\theta}{c}\frac{d}{dx}(E_w c_g \cos\theta + 2E_r c\cos\theta) \tag{2.19}$$

2.2.2. Current modelling

The current in alongshore direction is determined by the alongshore momentum equation. The above current driving force (Eq (2.19)) is balanced by bottom friction and lateral friction. In the present model, a depth-averaged mode is considered.

The bottom friction stress is determined by the quadratic law:

$$\tau_b = \rho C_f < V|\vec{U}| > \tag{2.20}$$

where V is depth-averaged longshore current velocity, $\vec{U}$ is the instantaneous total horizontal velocity vector and C_f is a friction coefficient:

$$C_f = \frac{g}{C^2} \tag{2.21}$$

$$C = 18log\left(\frac{12h}{k_s}\right) \tag{2.22}$$

When the current velocity is much smaller compared to the wave orbital velocity, the bottom friction stress τ_b can be linearized by the following equation (Liu and Dalrymple, 1978)

$$\tau_b = \frac{2}{\pi}\rho C_f u_m V(1 + \sin^2\theta) \tag{2.23}$$

where u_m is total velocity variance.

The parametrisation of $<V|\vec{U}|>$ for random waves adopts the formulation of Wright and Thompson (1983) in an empirical form is

$$<V|\vec{U}| > = \sigma_t V\left(\alpha^2 + \left(\frac{V}{\sigma_t}\right)^2\right)^{\frac{1}{2}} \tag{2.24}$$

Where α is a coefficient, the best fit for α is 1.16 by (Feddersen et al., 2000).

The wave-averaged and depth-integrated longshore momentum equation governing the longshore current is

$$\tau_b = F_y + \rho\frac{dh\tau_{xy}}{dx} \tag{2.25}$$

where τ_{xy} is the horizontal turbulent stress.

$$\tau_{xy} = \nu_t \frac{dV}{dx} \tag{2.26}$$

where ν_t is the eddy viscosity.

2.3. Laboratory experiments

2.3.1. Visser (1991) experiments

Visser (1991) conducted a series of experiments to measure the spatial distribution of wave-induced longshore currents. To achieve a uniformity of the longshore current in the wave basin, Visser (1991) used a pumped recirculation in the experiments and fine-tuned the optimal recirculation discharge to minimize the return flow. The high quality control makes these experimental data one of the most popular calibration and/or validation sets for numerical models. Two cases of these experiments confined to regular waves and a 1:20 slope with a smooth concrete bottom were simulated, viz. Case 4 and Case 5 of Visser (1991) experiments (in short V91_C4 and V91_C5, respectively) The wave parameters are summarised in Table 1. The subscript "1" refers to values at the wave generators. The cross-shore profile is shown in Fig. 1, (a).

2.3.2. Hamilton et al. (2001) experiments

Another suitable data set of measured wave-induced longshore current for validation was produced by Hamilton and Ebersole (2001) in the wave basin of the Large-scale Sediment Transport Facility (LSTF). The smooth concrete beach slope was 1/30 (Fig. 1, b). Case 6N with regular waves was simulated. Similar to Visser (1991), a multiple pumping system was utilised to optimise the uniformity of longshore current.

2.3.3. Hulsbergen et al. (1973) experiments

Although the purpose of the H73 experiments was to investigate the interaction between pile screen groins and a wave-driven longshore

Table 1
The parameters of the experiments.

Exp.	wave	H_1 (m)	T_1 (s)	Θ_1 (^{0})	m	d_1 (m)	L_1 (m)	H_1/L_1	H_1/d_1	k_1 d_1	Beach type
V91_C4	Regular	0.078	1.02	15.4	1:20	0.350	1.46	0.053	0.22	1.51	plane
V91_C5	Regular	0.071	1.85	15.4	1:20	0.350	3.19	0.022	0.20	0.70	plane
H01_6N	Regular	0.182	2.50	10.0	1:30	0.667	5.94	0.031	0.27	0.71	plane
H73_W	Regular	0.030	1.04	15.0	1:35	0.300	1.45	0.021	0.10	1.30	plane
R97_SA243	Regular	0.08	1.00	30.0	1:20	0.55	1.53	0.052	0.15	2.26	barred
R97_SO014	Irregular	0.07	1.20	30.0	1:20	0.55	2.09	0.034	0.13	1.65	barred

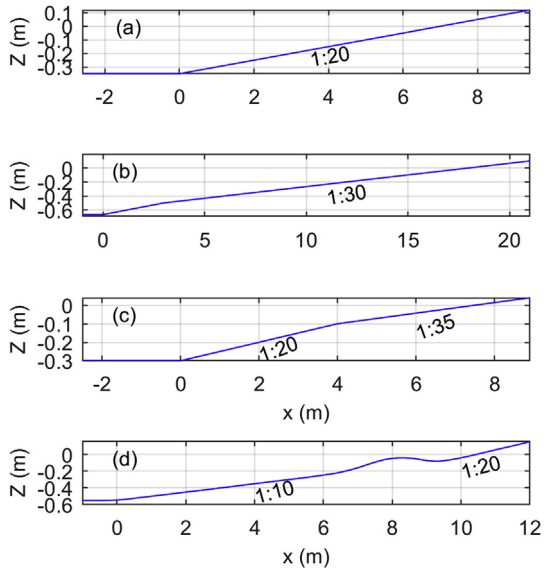

Fig. 1. The bottom profile of each experiment: (a), Visser (1991); (b), Hamilton and Ebersole (2001); (c), Hulsbergen and ter Horst, 1973; (d) Reniers and Battjes (1997).

current, the base case without groins provides an additional valuable, validation/calibration data set. The wave only experiment was conducted in a wave basin of Delft Hydraulics. The bottom contours are straight and parallel to the shoreline. Regular waves with H = 0.03 m and T = 1.04 s were generated approaching the shore at an incidence angle of 15 ^{0}.

2.3.4. *Reniers and Battjes (1997) experiments*

Reniers and Battjes (1997) conducted laboratory experiments for wave driven longshore currents on barred and non-barred beaches. As the above mentioned four cases are all about plane beaches, two tests with a barred beach (Fig. 1, d), test SA243 under regular waves and test SO014 under irregular waves, were chosen to be reproduced. The height of the bar is about 10 cm, of which the inner slope is 1:8. The plane slope of the beach seaward is 1:10 while the shoreward slope is 1:20. The water depth at the wave maker is 0.55 m. The wave parameters are listed in Table 1.

3. Results

3.1. *V91 experiments*

To verify the ability of the SWASH model in simulating wave-induced longshore currents, a set of numerical simulations was conducted to compare to Case 4 and Case 5 of the Visser (1991) experiments. The number of vertical layers was set at 20, which is fine enough to resolve the flow vertical structure. To achieve a more efficient computation time, the so-named subgrid method (Rijnsdorp et al., 2017) was applied to derive the vertical accelerations and pressure gradients on a coarser grid of 4 layers. The remaining wave and mean flow dynamics are resolved on the fine grid. Such a two-grid system reduces computational efforts substantially by an order of magnitude. The validation of the subgrid approach showed that the predictions by subgrid simulations are comparable to that of fully resolved simulations (Rijnsdorp et al., 2017).

3.1.1. *Case 4*

For Case 4 of V91 experiments, the time step was set at $\Delta t = 0.005$ s, the grid resolution was set $\Delta x = 0.03$ m in cross-shore direction and $\Delta y = 0.044$ m in alongshore direction (400 × 128 grid cells in total). The obliquely incident regular waves with a period of 1.02 s, an amplitude of 0.039 m and an incident angle of 15.4^0, were generated at the offshore boundary. A periodic boundary was used at the lateral boundaries to limit the length of an unbounded beach. In the laboratory experiment, the bottom was made of smooth concrete. The roughness height value of a smooth concrete bottom is suggested as 0.001 m by Visser (1984a,b), 0.0005 m by Reniers and Battjes (1997), and 0.0004 m by Rijnsdorp et al. (2017). Hereinafter, the roughness height was chosen at ks = 0.0005 m for this following cases as a default setting which is qualified as validation and not calibration, since it is well within the default range.

After a computational duration of 150 s, the current field reaches a stationary state as demonstrated in Fig. 2, indicating that the differences between the longshore current profiles at t = 120 s and t = 150 s are relatively small. In Fig. 3, the computed instantaneous water level and the phase- and depth-averaged current field are shown. As waves approach the shore, waves are transforming due to shoaling effects and changing direction because of depth refraction. Then wave heights start to decrease once depth limited breaking occurs. It is clearly shown that there is a spatial lag between the location of maximal horizontal current velocity and that of the maximal wave height.

The cross-shore variations of wave height, mean water level and longshore current are shown in Fig. 4. The blue lines denote the computed results, while the red circles are the measured V91 data. The simulation successfully captures the right location of wave breaking point. The waves start to break at x = 5 m, 2 m offshore to the shoreline at x = 7 m. The wave heights are slightly overpredicted within the surf zone, which suggests that the model may slightly underestimate the

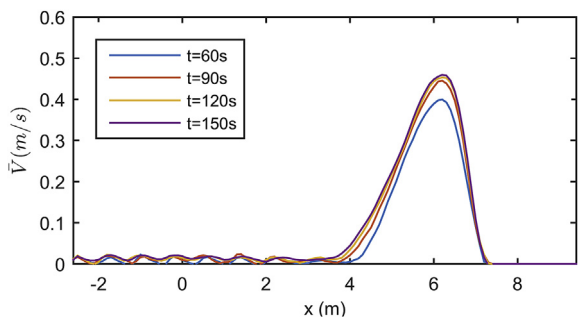

Fig. 2. The cross-shore profile of computed longshore current at t = 60 s (blue line), t = 90 s (red line), t = 120 s (yellow line), t = 150 s (purple line). (For interpretation of the references to colour in this figure legend, the reader is referred to the Web version of this article.)

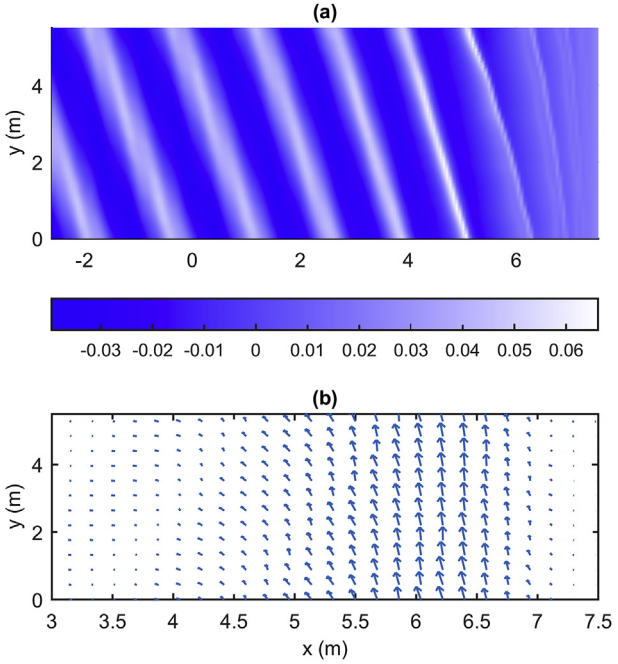

Fig. 3. Case 4 (H = 0.078 m, T = 1.02 s, θ = 15.4^0) of V91 experiments; (a) snapshot of the computed wave field (the unit of the colour bar is m) and (b) the phase-averaged and depth-averaged current field. (For interpretation of the references to colour in this figure legend, the reader is referred to the Web version of this article.)

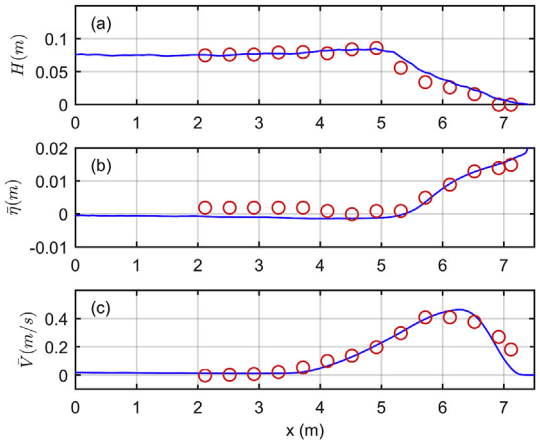

Fig. 4. Case 4 of V91 experiments; the cross-shore distribution of wave height (a), wave set up (b) and longshore current velocity (c), (blue lines: simulations, red circles: measurements). (For interpretation of the references to colour in this figure legend, the reader is referred to the Web version of this article.)

energy dissipation rate. This observed deviation is similar to the results of the same case simulated by Chen, 2003, who found the same over-prediction using a phase-resolving Boussinesq type model. Nevertheless, the computed wave set up and longshore current velocity agree very well with the measured data. The slight overestimation of the wave set up is consistent with the trend of the computed wave height, and may be partly due to a minor underestimation of the longshore current velocity.

As shown in Fig. 4 c, the model quite accurately predicts the cross-shore variation of the longshore current as well as the location and magnitude of the maximum velocity. Overall, the well-matched results reveal the validity of the wave-breaking scheme and of the transformation of momentum flux in both longshore and cross-shore directions.

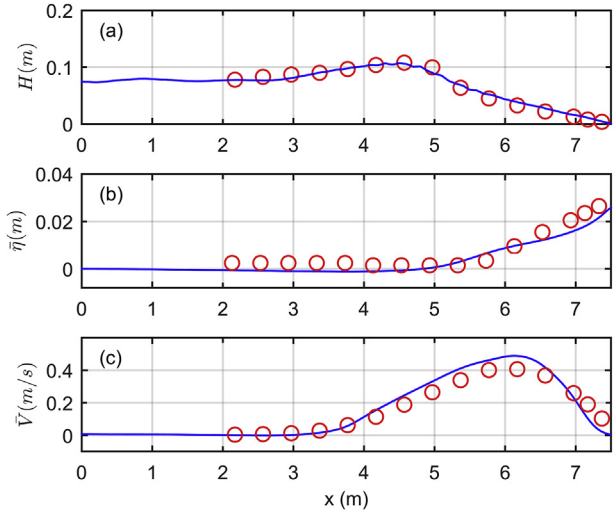

Fig. 5. Case 5 (H = 0.071 m, T = 1.85 s, θ = 15.4^0) of V91 experiments; the cross-shore distribution of wave height (a), wave set up (b) and longshore current velocity (c), (blue lines: simulations, red circles: measurements). (For interpretation of the references to colour in this figure legend, the reader is referred to the Web version of this article.)

3.1.2. Case 5

For this case, with a longer wave period of 1.85 s, the grid resolution could be increased to Δx = 0.05 m and Δy = 0.087 m (resulting in 240 × 140 grid cells in total). Other parameters are kept the same as in Case 4. The computed wave height is nearly the same as the measured data (Fig. 5). The waves started to break at x = 4.5 m, 2.5 m offshore to the shoreline at x = 7 m. Although the longshore current velocity is slightly overestimated, its cross-shore profile is well reproduced.

3.2. H01_6N experiment

In this simulation the time step was set at Δt = 0.005 s, the grid resolution was set Δx = 0.08 m and Δy = 0.16 m (275 × 225 grid cells in total). The roughness height was set at ks = 0.0005 m, the same as the default value. The number of vertical layers was set at 20, which is found fine enough to resolve the vertical variation of mean flow structure from previous simulation experience, while the coarse subgrid with 4 pressure layers was turned on.

The comparable simulation results with the measurement data are shown in Fig. 6. The simulation accurately reproduces the wave height transformation. The finer resolution of the numerical model predicts the wave breaking point at x = 10.5 m, while the measured maximal wave height is at x = 9.48 m and the next measurement point is beyond 10.5 m. The wave height variation cross-shore shows a good agreement with the observed values (Fig. 6, (a)). Both the locations of the wave set-up and the maximal longshore current are accurately computed. Similarly to the V91_C4 simulation, within the surfzone, the wave set-up is slightly overestimated while the longshore current is slightly underestimated. This pattern of deviations between simulations and measurements of H01_6N and V91_C4 experiments may be due to their more similar wave steepness.

3.3. H73_W experiment

In addition to the above validations against the well-known V91 and H01 experiments, a unique, not well-known, but valuable data set is obtained from (Hulsbergen and ter Horst, 1973). As part of their comprehensive measurements of the impact of groins on the longshore current, here their wave only case is used for additional validation.

To reproduce the experiments numerically, the time step was set at Δt = 0.005 s, the grid resolution was set Δx = 0.03 m and

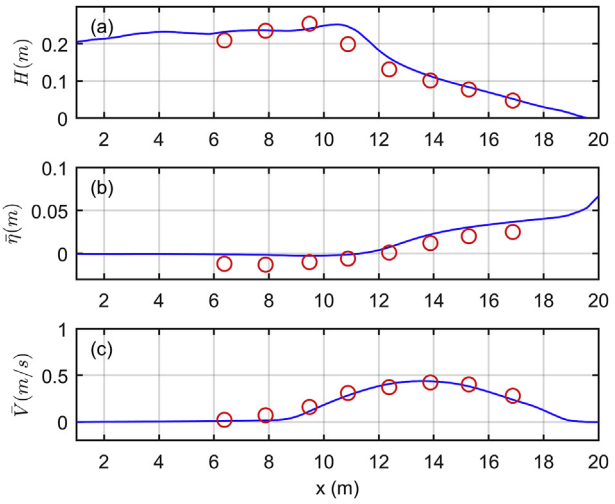

Fig. 6. Case H01_6N (H = 0.182 m, T = 2.5 s, θ = 10^0); the cross-shore distribution of wave height (a), wave set up (b) and longshore current (c), (blue lines: simulations, red circles: measurements). (For interpretation of the references to colour in this figure legend, the reader is referred to the Web version of this article.)

Δy = 0.044 m (resulting in 380 × 128 grid cells). The roughness height was set at ks = 0.0005 m, again in the default range. The vertical velocity layers were chosen 20 while the coarse pressure layers were 4.

For this condition, the computed maximal alongshore velocity is 0.14 m/s at x = 6.5 m (Fig. 7c). The mean longshore current velocities show satisfactory agreement with the measured data, but the velocities are slightly underestimated. Because of the crude assumption that the vertical profiles of the longshore currents within the surf zone are uniform, the measured velocities by float points in the upper water column might need to be interpreted as depth-averaged velocities, which may partially explain the underestimation. The calculated breaker point is at about x = 5.5 m (Figs. 7a), 2 m seaward to the shoreline at x = 7.5 m, consistent with the observation in the experiment (Hulsbergen and ter Horst, 1973). Wave heights and set-up were not measured, but as the longshore current velocities are much more sensitive to the parameters than the wave heights and mean water level, we have confidence that the simulated wave heights and mean water

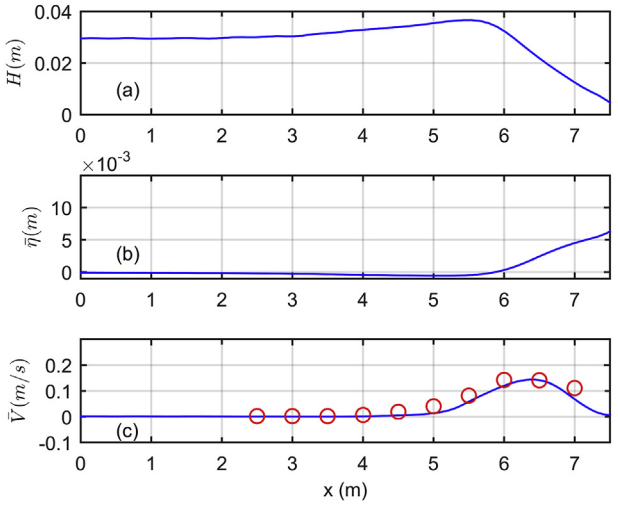

Fig. 7. Case H73_W (H = 0.03 m, T = 1.04 s, θ = 15^0); the cross-shore distribution of wave height (a), wave set up (b) and longshore current (c), (blue lines: simulations, red circles: measurements). (For interpretation of the references to colour in this figure legend, the reader is referred to the Web version of this article.)

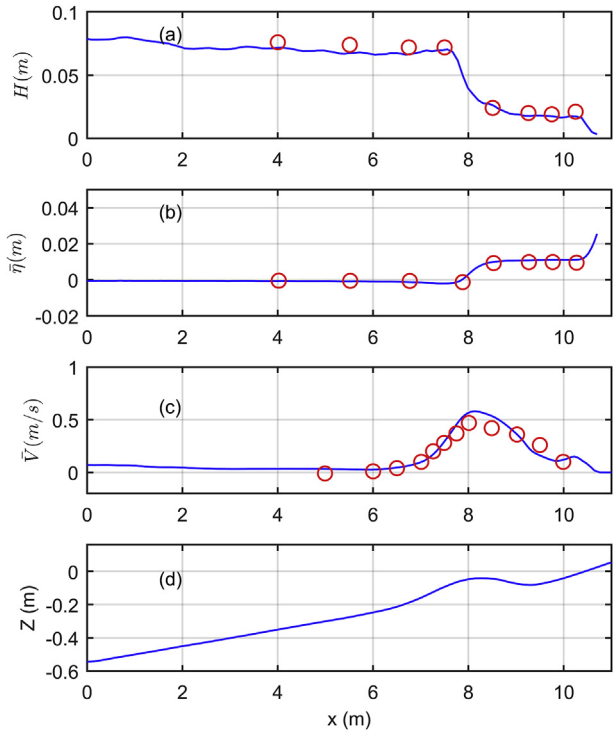

Fig. 8. Case R97_SA243 (H = 0.08 m, T = 1 s, θ = 30^0); the cross-shore distribution of wave height (a), wave set up (b), longshore current (c) and the bottom profile (d), (blue lines: simulations, red circles: measurements). (For interpretation of the references to colour in this figure legend, the reader is referred to the Web version of this article.)

level are accurate. The computed maximum wave set-up reaches a value of 0.0092 m, which is approximately equal to 0.0075 m computed from linear wave theory.

3.4. R97 experiments

3.4.1. Case SA243

As the above all cases are about plane beaches, a more complex barred slope, of the experiment SA243 conducted by Reniers and Battjes (1997), was considered. The case Re97_SA243 was simulated and compared with experimental data. The numerical domain consists of 440 grids (Δx = 0.03 m) in cross-shore direction and 100 grids (Δy = 0.031 m) in alongshore direction. Other parameters and settings are the same as the default.

It is shown (Fig. 8) that the locations of the wave breaking, wave set down and maximal longshore current are all accurately calculated. The waves were starting breaking on the outer bar slope when the water depth is rapidly reduced. Then the spatially lagged maximal longshore current appeared on the bar crest. The observed bimodal shape of longshore current was also reproduced, where one peak location is at the bar crest and the other peak is near the shoreline. The second peak was not measured but visually observed by dye movement in the experiment due to that the limited water depth (< 3 cm) is beyond the usage range of measurement apparatuses (Reniers and Battjes, 1997).

3.4.2. Case SO014

Unlike the previous cases all tested under regular waves, case SO014 was tested with irregular waves. The numerical grid resolution is Δx = 0.041 m in cross-shore direction and Δy = 0.084 in alongshore direction. Other parameters and settings are kept the same as previous simulations. Again, a good agreement between modelled and measured longshore current velocities was obtained (Fig. 9).

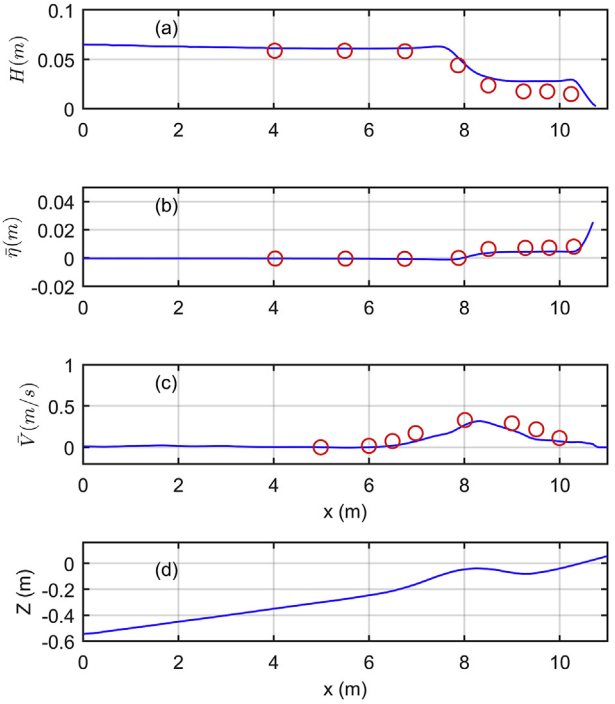

Fig. 9. Case R97_SO014 (Hs = 0.07 m, Tp = 1.2 s, θ = 30⁰); the cross-shore distribution of wave height (a), wave set up (b), longshore current (c) and the bottom profile (d), (blue lines: simulations, red circles: measurements). (For interpretation of the references to colour in this figure legend, the reader is referred to the Web version of this article.)

3.5. Analysis of modelled longshore currents

To evaluate the performance of the SWASH model, three statistical parameters, i.e. root mean square error (RMSE), relative bias (the sum of errors over the sum of observed values) and correlation coefficient (R^2) are computed for all six numerical simulations. The results are listed in Table 2. For both wave height and longshore current computations, the root mean square errors are confined to a relatively small value. All correlation coefficients are larger than 0.97, revealing a strong correlation between the simulated results and measurements. For the specific interest in modelling longshore currents of this study, comparisons between modelled and observed values are depicted in Fig. 10. The relative small RMSE and strong correlation coefficient validate the capacity of modelling longshore currents of SWASH with just default set parameters on both barred and non-barred beaches. However, the much larger relative bias of R97_SO014 shows that the swash model results are much worse for irregular waves than the results of other experiments under regular waves with default parameter settings.

Table 2
Statistics of the computed bulk parameters against the measurements.

H	RMSE (m)	R^2	Relative bias (%)
V91_C4	0.0086	0.9798	9,08
V91_C5	0.0056	0.9931	1,16
H01_6N	0.0188	0.9728	5,25
R97_SA243	0.0039	0.9968	−6,34
R97_SO014	0.0085	0.9948	20,30
$\bar{V}$	RMSE (m/s)	R^2	Relative bias (%)
V91_C4	0.0415	0.9700	−9,76
V91_C5	0.0348	0.9815	−11,33
H01_6N	0.0396	0.9871	−11,13
H73	0.0195	0.9707	−25,07
R97_SA243	0.0582	0.9593	5,55
R97_SO014	0.0703	0.9523	−38,69

3.6. Validated and predicted vertical variations of longshore currents

Given the availability of measurement data, only the vertical variations of longshore currents of experiment H01_6N could be validated (Fig. 11). The calculated longshore current velocities V(z) matched well with observed values at five different locations, except for an underestimation at the nearest location (X = 1.16 m offshore). From the furthest offshore location (X = 8.52 m offshore where h = 0.274 m) to the third nearest to shoreline location (X = 4.12 m offshore where h = 0.149 m), little vertical variations of the velocity profiles were observed (Fig. 11). Therefore, the vertical profiles can be characterised as depth uniform. At a further inshore location (X = 2.76 m), the turbulent bottom boundary layer becomes dominant, and the vertical profile changes from a rather depth uniform to a logarithmic profile.

To investigate the vertical variation of longshore current for the other five experiments, the depth variation of the predicted normalised longshore current $\bar{v}/c$ is illustrated in Fig. 12, where c is the local shallow wave celerity. The vertical profile locations in the figure are ranging from 0.4 to 1.4 times the width of the surf zone, increasing at a 0.2 times width interval. At 1.4 times x_b, the longshore current is almost zero for all cases. Similarly, the normalised longshore currents reach their largest value halfway across the breaker zone on planar beaches of the first four experiments. Because of the stronger bottom friction near the shoreline, a slight deviation from a depth uniform profile arises, where the normalised longshore current at the upper water column is slightly larger than that near bottom. Further offshore, the profiles of the longshore current are nearly vertical, verifying that the longshore current is rather depth uniform within most breaker zones under regular waves on planar beaches.

The generally depth uniform trend is supported by similar observations in the Hamilton and Ebersole (2001) and Visser (1991) laboratory experiments, and in the Sandy Duck field experiments (Reniers et al., 2004). One possible reason would be the breaking wave induced turbulence injected downward, smoothing the vertical current profile (for instance, Fig. 1 in Svendsen and Lorenz, 1989, and Fig. 1 in Church and Thornton, 1993). Another possible reason would be the dispersive mixing by the interaction of mean longshore currents and cross-shore currents (Putrevu and Svendsen, 1993). Due to the strong influences of dispersion and turbulence on the vertical variations of longshore current profiles, the boundary layer would not be fully developed with the existence of breaking waves. It is shown that the generally depth uniform longshore current profile is confined to regular waves on planar beaches. When the other two experiments with a barred slope were considered (Fig. 12), it is found that the vertical profiles tend to be more uniform under random waves (Re97_SO014) than under regular waves (Re97_SA243). However, the vertical profiles of longshore currents are much more logarithmic over the bar.

3.7. SWASH model vs 1D model

If the very shallow zone is not considered and the vertical variation of the cross-shore current is not of interest, a simple 1D longshore momentum balance model is shown sufficient to compute the longshore current. This phase-averaged 1D model complemented, is used to test the H73_W experiment, Re97_SA243 and Re97_SO014 experiments, compared with the validated simulation by the SWASH model. To accurately predict the peaks in the cross-shore distribution of longshore current and wave setup and set down, the roller model developed by Dally and Brown (1995) is included. The additional roller model has been affirmed necessary to shift the computed maximum longshore current landward of the breaker point (Osiecki and Dally, 1996; Reniers, 1999), to bridge the deviation of the numerical models from the measurements (Visser, 1984a,b; Reniers and Battjes, 1997).

The calculated results of the H73_W experiment are shown in

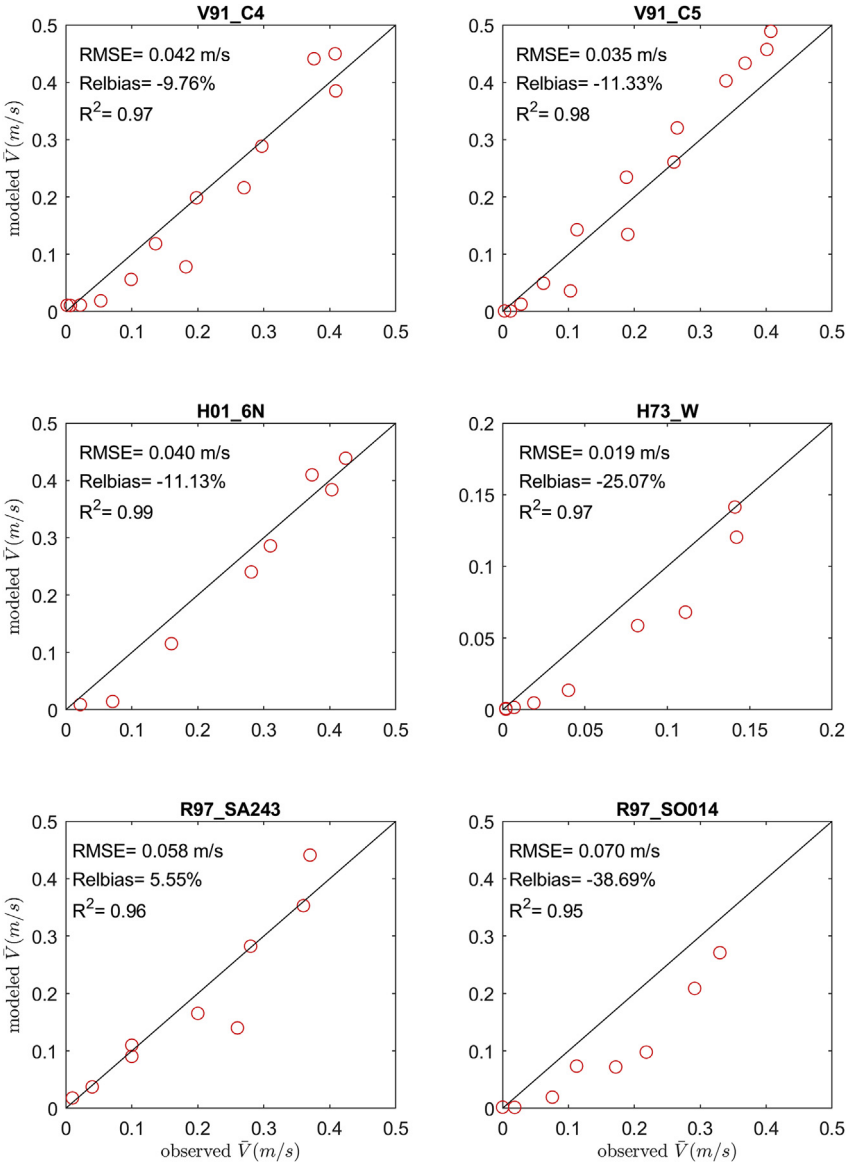

Fig. 10. Comparison of modelled and observed longshore current velocities for each experiment showing RMSE, Bias, and R^2 values. Black solid lines represent perfect agreement.

Fig. 13. For the 1D model, the wave set up is the most insensitive to the free parameters. In contrast, wave height is sensitive to the wave breaker index γ and the wave breaking fraction parameter B. The well calibrated γ is found to be 0.78. The value 1.75 of B is used which is the optimal value obtained by fitting to a laboratory data set (Power et al., 2013). Besides, the variation of the wave front angle β of the roller model and the viscosity dominate the cross shore profile of the longshore current. The value of β is chosen 0.1 while the eddy viscosity is taken as 0.01 m^2/s. The bottom roughness height, which significantly affects the magnitudes of longshore current velocities, was calibrated to be 0.0015 m. The calibrated bottom roughness value used in the 1D model is three times the recommended empirical value 0.0005 m used in the SWASH model.

In Fig. 14, the 1D model provides good results for the Re97_SA243 experiment on a barred slope under regular waves, when the bottom roughness height increased to 0.01 m. For the experiment Re97_SO014 on the same slope but under irregular waves, a good agreement was obtained (shown in Fig. 15) when the roller slope parameter was changed from 0.1 to 0.05, and the bottom roughness height 0.0005 m was used.

4. Discussion

The ability of the SWASH model in simulating longshore currents has been investigated and validated on barred and non-barred beaches under obliquely incident regular and irregular waves. Since the purpose of this study is to validate the SWASH model with uncalibrated default free parameters, the parameters (e.g. bottom roughness height, horizontal eddy viscosity) were set the same for all the simulation cases. Without any variation of the free parameters, the SWASH model provided promising results. It can be expected that after calibration, the accuracy of the SWASH model could even be improved. For instance, calibrating bottom friction coefficients would significantly affect modelled longshore current magnitudes, for which there is a large variability found in the literature.

The simulation results of the longshore currents on a barred slope (Re97_SA243 and Re97_SO014) are consistent with that measured in the laboratory. Confined to a well-controlled laboratory environment, both the modelled and observed longshore currents have the same cross-shore variations. The pattern is that the maximal longshore current occurs where the wave breaking induced turbulence is the

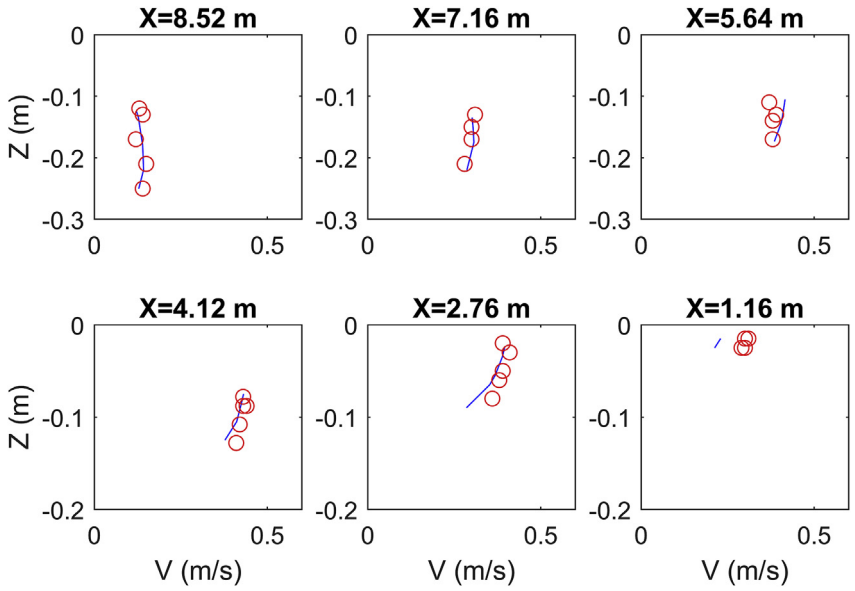

Fig. 11. Case H01_6N, the comparison of modelled and observed vertical variations of V(z), (blue line: simulation, red circle: measurement). (For interpretation of the references to colour in this figure legend, the reader is referred to the Web version of this article.)

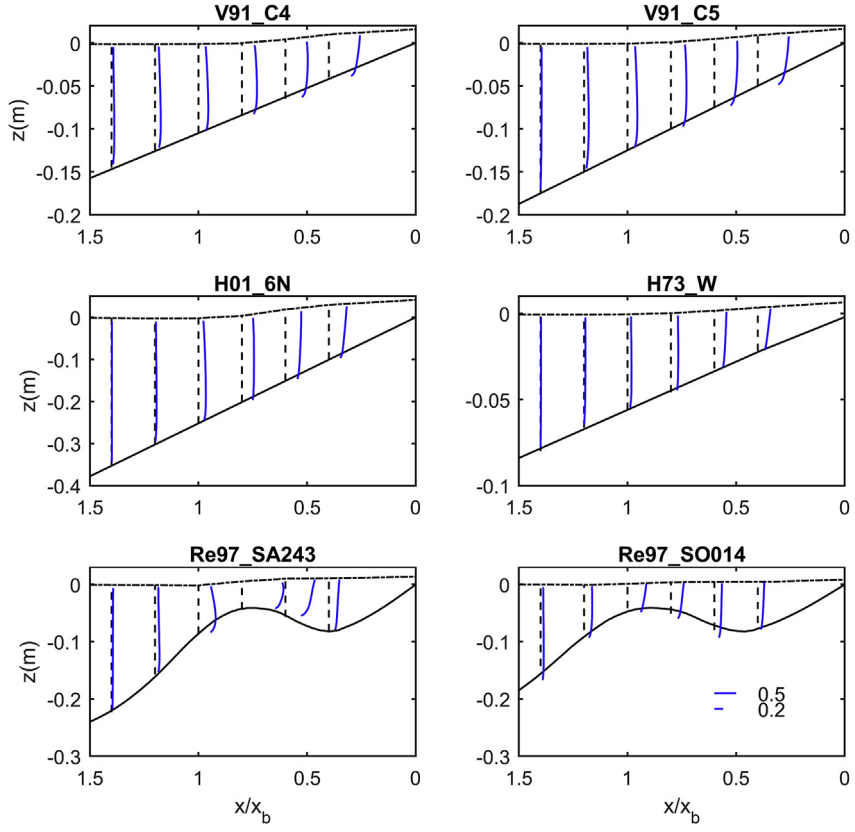

Fig. 12. The vertical profiles of normalised longshore shore current $\bar{v}/c$, $c(=\sqrt{gd})$ is local wave celerity. The vertical black dash line denotes the vertical profile location and indicates the zero value of each vertical profile of $\bar{v}$ /c (blue line). The dash dot and solid black lines represent the mean water level and slope bottom, respectively. The scale is given in Re97_SO014 figure. (For interpretation of the references to colour in this figure legend, the reader is referred to the Web version of this article.)

strongest. The second peak velocity appears near the shoreline. However, the field experiment DELILAH shows that the maximum longshore current velocity is on the trough but not over the bar crest. Reniers and Battjes (1997) attempted to test the effects of alongshore variation and lateral mixing of their numerical model on the position of the maximum. However, neither an alongshore pressure gradient nor lateral mixing significantly affects the maximum longshore current velocity position. It was concluded that the maximal longshore current velocities observed in the trough are not attributed to the pure local wave forcing (Reniers and Battjes, 1997). The deviation of observed and predicted maximum velocity position may due to the failure to identify the alteration of the local forcing mechanism (Church and

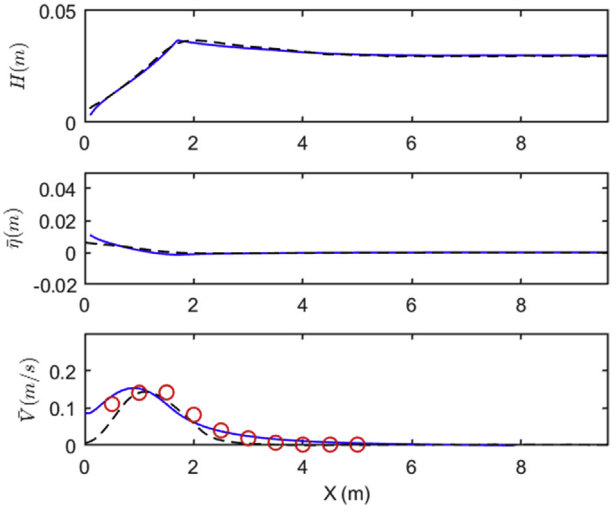

Fig. 13. Comparison between the simulated results of the H73_W experiment by the 1D model (blue line) and the results obtained by the SWASH model (black dash line), (red circles: measurements). (For interpretation of the references to colour in this figure legend, the reader is referred to the Web version of this article.)

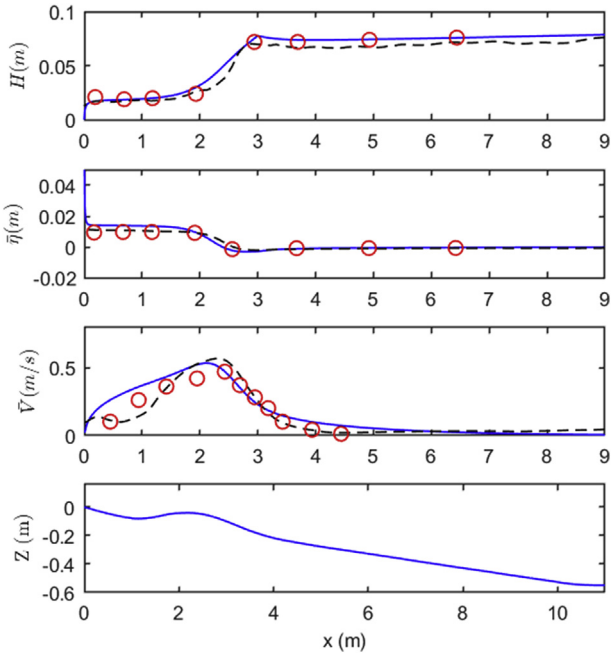

Fig. 14. Comparison between the simulated results of the R97_SA243 experiment by the 1D model (blue line) and the results obtained by the SWASH model (black dash line), (red circles: measurements). (For interpretation of the references to colour in this figure legend, the reader is referred to the Web version of this article.)

Thornton, 1993). For complex forces (e.g. wind and tidal effects) in the field environment was not considered in the laboratory experiments and the numerical simulations by the SWASH model except for pure wave forces, the SWASH model could only reproduce the laboratory experiment results well, but could not contribute to illuminating the possible reason why the observed positions of maximal longshore currents appear in the trough.

It is shown that a simple 1D model is able to compute a longshore current distribution comparable to the SWASH model. However, the bottom roughness coefficient dominates the magnitude of computed longshore current velocity, of which the realistic value is not optimum

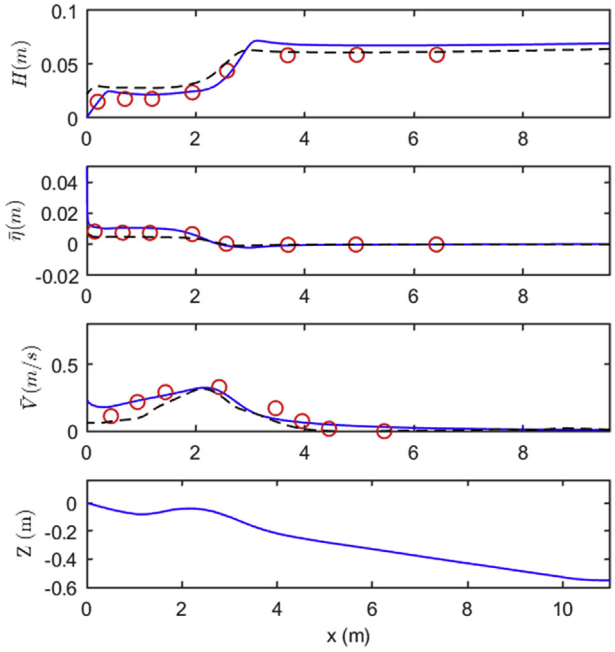

Fig. 15. Comparison between the simulated results of the R97_SO014 experiment by the 1D model (blue line) and the results obtained by the SWASH model (black dash line), (red circles: measurements). (For interpretation of the references to colour in this figure legend, the reader is referred to the Web version of this article.)

all the time and then needs a calibration. For instance, the calibrated bottom roughness height varies a factor of twenty for the simulations on a barred slope. In addition, the cross-shore distribution of the longshore current depends on the eddy viscosity value in order to mimic the horizontal momentum flux diffusion, which is generally unknown. Different correlations between the eddy viscosity, characteristic length scale (i.e. wave height or water depth), and characteristic velocity (i.e. wave celerity or turbulent velocity) are available in the literature (i.e. Longuet-Higgins, 1970b; Battjes. J.A., 1975, Putrevu and Svendsen, 1993). The simplest constant eddy viscosity was used in the simulations with a calibration, instead of choosing an available eddy viscosity model. While this finding illustrates the dominant mechanism for the generation of the longshore current distribution, the uncertainty of the free parameter value limits the prediction ability of the 1D model. Compared to the 1D model, the SWASH model is more accurate without having to pay attention to tuning the free parameters. When the vertical resolution is fine enough to resolve the vertical structure of mean flow, the order of O(20) in this study, and the computational domain is properly long with minor lateral boundary effects, the SWASH model reproduces the longshore current profiles in laboratory experiments fairly well, while only proper magnitude of longshore current velocity could be predicted by the 1D model. Therefore, the SWASH model with default parameter settings is suggested to predict the distribution of longshore currents accurately.

5. Conclusions

The SWASH model has been set up to simulate wave induced current against six laboratory experiments, four of which are confined to obliquely incident regular waves on non-barred beaches, and two experiments are on a barred beach under regular waves and irregular waves respectively. Nearly perfect agreements are found between the computed and measured wave heights, mean water levels and longshore currents. The longshore current generally spreads within 2 times the surf zone width (Longuet-Higgins,1970b). For simpler well-controlled experiments with regular wave incidence to alongshore uniform

beaches considered in this paper, the longshore current is shown to develop mostly within 1.5 times the width of the surf zone. Along vertical direction, the longshore current is quite depth uniform on plane beaches. The exception, existing in very shallow water, is that the vertical profile of longshore current deviates from a depth uniform profile. The stronger bottom friction in shallower water enforces the vertical profile to transform into a logarithmic profile. Ignoring the vary shallow zone nearshore, approximately stretching over 0.4 times surf zone width offshore, longshore currents maybe assumed depth uniform under regular waves on plane beaches. Both the numerical simulations and laboratory measurements show rather depth uniform vertical structure of mean longshore current under regular waves on plane beaches. This explains partly why the simpler 1D depth-averaged momentum balance equation can be sufficient to compute the longshore current. However, the assumption of depth uniform longshore current does not apply to a bared beach.

In conclusion, the phase-resolving SWASH model is capable to compute wave-induced longshore currents. The subgrid approach accelerates the computation without sacrificing the accuracy. The less computational effort shows that this phase-resolved model is a promising alternative to a phase-averaged model. Without tuning effort on free parameters, the SWASH model predicts wave generated longshore current fairly well on planar and barred beaches. More complex conditions such as combined wave and steady current condition, or realistic random waves in combination with tidal currents in fields would be investigated in further work.

Acknowledgements

The first author is sponsored by the Chinese Scholarship Council (grant number: 201406060020). We gratefully thank Dr. Hulsbergen and Dr. Visser for their explanations about their experiments and Dr. Rijnsdorp for sharing his professional expertise in SWASH modelling. Finally, the suggestions and advice from the reviewers, Professor Baldock and two anonymous reviewers, are very appreciated which helped to improve this paper.

Appendix A. Supplementary data

Supplementary data to this article can be found online at https://doi.org/10.1016/j.coastaleng.2018.10.005.

References

Battjes, J.A., 1975. Modelling of turbulence in the surfzone. In: Proc. Symp. Model. Techniques. San Francisco, CA, pp. 1050–1061.
Bowen, A., 1969. The generation of longshore currents on a plane beach. J. Mar. Res. 27, 206–215.
Chen, Q., 2003. Boussinesq modeling of longshore currents. J. Geophys. Res. 108, 3362. https://doi.org/10.1029/2002JC001308.
Church, J.C., Thornton, E.B., 1993. Effects of breaking wave-induced turbulence within a longshore-current model. Coast. Eng. 20, 1–28.
Dally, W.R., Brown, C.A., 1995. A modeling investigation of the breaking wave roller with application to cross-shore currents. J. Geophys. Res. 100, 24873–24883. https://doi.org/10.1029/95JC02868.
de Bakker, A.T.M., Tissier, M.F.S., Ruessink, B.G., 2016. Beach steepness effects on nonlinear infragravity-wave interactions: a numerical study. J. Geophys. Res. Ocean. 121, 554–570. https://doi.org/10.1002/2015JC011268.
Duncan, J.H., 1981. An experimental investigation of breaking waves produced by a towed hydrofoil. Proc. R. Soc. A Math. Phys. Eng. Sci. 377, 331–348. https://doi.org/10.1098/rspa.1981.0127.
Feddersen, F., Guza, R.T., Elgar, S., Department, T.H.C.H., 2000. Velocity moments in alongshore bottom stress parameterizations. J. Geophys. Res. 105, 8673–8686.
Galvin, C.J., Eagleson, J.P.S., 1964. Experimental Study of Longshore Currents on a Plane Beach. Hydrodynamics Laboratory Report, vol. 63 Massachusetts Institute of Technology, Cambridge.
Hamilton, D.G., Ebersole, B.A., 2001. Establishing uniform longshore currents in a large-scale sediment transport facility. Coast. Eng. 42, 199–218. https://doi.org/10.1016/S0378-3839(00)00059-4.
Hsu, C.-E., Hsiao, S.-C., Hsu, J.-T., 2017. Parametric analyses of wave-induced nearshore current system. J. Coast Res. 33, 795–801. https://doi.org/10.2112/JCOASTRES-D-16-00027.1.
Hulsbergen, C.H., ter Horst, W., 1973. Effect of Permeable Pile Screens on Coastal Currents, vol. M1148 Delft Hydraulics laboratory report, Delft (in Dutch).
Launder, B.E., Spalding, D.B., 1974. The numerical computation of turbulent flows. Comput. Methods Appl. Mech. Eng. 3, 269–289. https://doi.org/10.1016/0045-7825(74)90029-2.
Liu, P.L.-R., Dalrymple, R.A., 1978. Bottom frictional stresses and longshore currents due to waves with large angles of incidence. J. Mar. Res. 36, 357–375.
Longuet-Higgins, M.S., 1970a. Currents generated by obliquely incident sea waves: 1. J. Geophys. Res. 75, 6778–6789.
Longuet-Higgins, M.S., 1970b. Longshore current generated by obliquely incident sea waves: 2. J. Geophys. Res. 75, 6790–6801.
Longuet-Higgins, M.S., Stewart, R.W., 1964. Radiation stresses in water waves; a physical discussion, with applications. Deep Sea Res. 11, 529–562.
Osiecki, D., Dally, W., 1996. The influence of rollers on longshore currents. In: 25th International Conference on Coastal Engineering. Orlando, pp. 3419–3430.
Power, H.E., Baldock, T.E., Callaghan, D.P., Nielsen, P., 2013. Surf zone states and energy dissipation regimes — a similarity model. Coast Eng. J. 55, 1350003. https://doi.org/10.1142/S0578563413500034.
Putrevu, U., Svendsen, I. a., 1992. A mixing mechanism in the nearshore region. In: 23rd International Conference on Coastal Engineering. Venice, pp. 2758–2771. https://doi.org/10.1061/9780872629332.210.
Reniers, a. J.H.M., Battjes, J. a., 1997. A laboratory study of longshore currents over barred and non-barred beaches. Coast. Eng. 30, 1–22. https://doi.org/10.1016/S0378-3839(97)00017-3.
Reniers, a. J.H.M., Thornton, E.B., Stanton, T.P., Roelvink, J. a., 2004. Vertical flow structure during Sandy Duck: observations and modeling. Coast. Eng. 51, 237–260. https://doi.org/10.1016/j.coastaleng.2004.02.001.
Reniers, A., 1999. Longshore Current Dynamics. Delft University of Technology.
Rijnsdorp, D.P., Smit, P.B., Zijlema, M., 2014. Non-hydrostatic modelling of infragravity waves under laboratory conditions. Coast. Eng. 85, 30–42. https://doi.org/10.1016/J.COASTALENG.2013.11.011.
Rijnsdorp, D.P., Smit, P.B., Zijlema, M., Reniers, A.J.H.M., 2017. Efficient non-hydrostatic modelling of 3D wave-induced currents using a subgrid approach. Ocean Model. 116, 118–133. https://doi.org/10.1016/j.ocemod.2017.06.012.
Smagorinsky, J., 1963. General circulation experiments with the primitive equations. Mon. Weather Rev. 91, 99–164. https://doi.org/10.1175/1520-0493(1963)091<0099:GCEWTP>2.3.CO;2.
Smit, P., Zijlema, M., Stelling, G., 2013. Depth-induced wave breaking in a non-hydrostatic, near-shore wave model. Coast. Eng. 76, 1–16. https://doi.org/10.1016/J.COASTALENG.2013.01.008.
Smith, J.M., Larson, M., Kraus, N.C., 1993. Longshore current on a barred beach: field measurements and calculation. J. Geophys. Res. Ocean. 98, 22717–22731. https://doi.org/10.1029/93JC02116.
Stive, M.J.F., 1984. Energy dissipation in waves breaking on gentle slopes. Coast. Eng. 8, 99–127.
Stive, M.J.F., De Vriend, H.J., 1994. Shear stresses and mean flow in shoaling and breaking waves. In: 24th International Conference on Coastal Engineering. Kobe, pp. 594–608.
Suzuki, T., Altomare, C., Veale, W., Verwaest, T., Trouw, K., Troch, P., Zijlema, M., 2017. Efficient and robust wave overtopping estimation for impermeable coastal structures in shallow foreshores using SWASH. Coast. Eng. 122, 108–123. https://doi.org/10.1016/j.coastaleng.2017.01.009.
Svendsen, I. a., Lorenz, R.S., 1989. Velocities in combined undertow and longshore currents. Coast. Eng. 13, 55–79. https://doi.org/10.1016/0378-3839(89)90032-X.
Svendsen, I.A., 1984. Wave heights and set-up in a surf zone. Coast. Eng. 8, 303–329.
Svendsen, I.A., Putrevu, U., 1994. Nearshore mixing and dispersion. Proc. Math. Phys. Sci. 445, 561–576. https://doi.org/10.1080/037454809495909.
Thornton, E.B., Guza, R.T., 1986. Surf zone longshore currents and random waves: field data and models. J. Phys. Oceanogr. 16, 1165–1178. https://doi.org/10.1175/1520-0485(1986)016<1165:SZLCAR>2.0.CO;2.
Thornton, E.B., Guza, R.T., 1983. Transformation of wave height distribution. J. Geophys. Res. 88, 5925. https://doi.org/10.1029/JC088iC10p05925.
Visser, P.J., 1991. Laboratory measurements of uniform longshore currents. Coast. Eng. 15, 563–593. https://doi.org/10.1016/0378-3839(91)90028-F.
Visser, P.J., 1984a. Uniform longshore current measurement and calculations. In: 19th International Conference on Coastal Engineering. Houston, pp. 2192–2207.
Visser, P.J., 1984b. A mathematical model of uniform longshore currents and the comparison with laboratory data. In: Comm. on Hydraulics, Rep. 84-2, (Dep. Civil Eng., Delft Univ. of Technology, Delft, The Netherlands).
Visser, P.J., 1982. The Proper Longshore Current in a Wave Basin. pp. 82–91 Delft, the Netherlands. Rep.
Visser, P.J., 1980. Longshore current flows in wave basin. In: 17th International Conference on Coastal Engineering. Sydney, pp. 462–479.
Wright, D.G., Thompson, K.R., 1983. Time-averaged forms of the nonlinear stress law. J. Phys. Oceanogr. 13, 341–345. https://doi.org/10.1175/1520-0485(1983)013<0341:TAFOTN>2.0.CO;2.
Zijlema, M., Stelling, G., Smit, P., 2011. SWASH: an operational public domain code for simulating wave fields and rapidly varied flows in coastal waters. Coast. Eng. 58, 992–1012. https://doi.org/10.1016/J.COASTALENG.2011.05.015.